NUMERICAL LINEAR ALGEBRA WITH APPLICATIONS
Numer. Linear Algebra Appl. 2013; **20**:645–662
Published online 11 April 2013 in Wiley Online Library (wileyonlinelibrary.com). DOI: 10.1002/nla.1882

On the convergence of shifted Laplace preconditioner combined with multilevel deflation

A. H. Sheikh*,†, D. Lahaye and C. Vuik

Delft Institute of Applied Mathematics, Delft University of Technology, Mekelweg 4, Delft, Netherlands 2628CD

SUMMARY

Deflating the shifted Laplacian with geometric multigrid vectors yields speedup. To verify this claim, we investigate a simplified variant of Erlangga and Nabben presented in [Erlangga and Nabben, ETNA, 2008;31:403–424]. We derive expressions for the eigenvalues of the two-level preconditioner for the one-dimensional problem. These expressions show that the algorithm analyzed is not scalable. They also show that the imaginary shift can be increased without delaying the convergence of the outer Krylov acceleration. An increase of the number of grid points per wavelength results in convergence acceleration. This contrasts to the use of the shifted Laplace preconditioner. Our analysis also shows that the use of deflation results in a spectrum more favorable to the convergence of the outer Krylov acceleration. The near-null space components are still insufficiently well resolved, and the number of iterations increases with the wavenumber. In the two-dimensional case, the number of near-zero eigenvalues is larger than in the one-dimensional case. We perform numerical computations with the two-level and multilevel versions of the algorithm on constant and nonconstant wavenumber problems. Our numerical results confirm our spectral analysis. Copyright © 2013 John Wiley & Sons, Ltd.

Received 6 January 2012; Revised 21 February 2013; Accepted 8 March 2013

KEY WORDS: Helmholtz equation; shifted Laplace preconditioner; multigrid deflation; Fourier analysis

1. INTRODUCTION

The aim of this work is to analyze a multilevel algorithm resembling the one presented in [1] for the iterative solution of the finite difference discretized Helmholtz equation with contrast in the wavenumber. The efficient solution of this problem has long been an open problem. It indeed appears that an increase of the wavenumber in almost all of the currently available solvers leads to a large increase in the number of iterations and therefore in computational cost. With the shifted Laplace preconditioner (SLP), the number of iterations increases linearly with the wavenumber. Alternative methods can be found in [2–5]. For a recent overview of preconditioners for the Helmholtz equation, we refer to [6].

The first papers on these preconditioners are [7] and [8] in which a Laplace operator and a Laplace operator with a real shift, respectively, are proposed. Both preconditioners lead to good results for medium-sized wavenumbers. For large wavenumbers, numerical results on the contrary show a steep increase in the number of iterations. A pioneering paper on SLPs is [9] in which incomplete LU decompositions of a shifted Laplace operator are used as a preconditioner. With the Laplace preconditioners with a complex shift proposed and studied in [10–12], the solver requires a number of iterations that grow only linearly as the wavenumber increases. Inspired by this work, a number

*Correspondence to: A. H. Sheikh, Delft Institute of Applied Mathematics, Delft University of Technology, Mekelweg 4, Delft, Netherlands 2628CD.

†E-mail: a.h.sheikh@tudelft.nl

of generalizations appeared shortly afterward in [1, 13–16] together with applications in different industrial contexts in [17–24]. More recent developments are given in [13, 25]. The convergence of the SLPs is analyzed in [26, 27]. This analysis shows that the smallest eigenvalues of the preconditioned operator rush to zero as the wavenumber increases and explains the nonscalability. In [1, 28], Erlangga and Nabben therefore propose to combine the SLP with deflation. As deflation vectors, the columns of the bilinear interpolation operator from coarse to fine grid are used. We will refer to these vectors as *multigrid vectors*. The deflation can be seen as a second-level preconditioner that attempts to remove small eigenvalues. The resulting method is quite involved and requires a flexible Krylov subspace method. Numerical results however suggest that the required number of iterations is nearly independent of the wavenumber.

In this paper, we analyze a simplified two-level variant of the method proposed in [1], referred to in the literature as ADEF-1 [29, 30]. In this algorithm, the SLP and the deflation operator are interpreted as a smoother and a coarse-grid correction step, respectively. We perform a rigorous Fourier two-grid analysis of one-dimensional and two-dimensional model problems with Dirichlet boundary conditions. In this analysis, both the smoother and the coarse-grid system are inverted by a direct method. Despite being a simplified setting, the one-dimensional analysis results in a closed-form expression for the eigenvalues of the two-grid operator that reveals the following three essential features of the solver. The deflation operator allows to make the SLP arbitrarily diagonally dominant by increasing the imaginary part of the shift without paying any penalty in the number of Krylov subspace iterations. It also shows that the performance of ADEF-1 improves if the number of grid points per wavelength is increased. Although it is well known that for the SLP the number of iterations for a fixed wavelength is mesh-width independent [26], a *reduction* of the number of iterations for the SLP in the limit of increasing the number of grid points per wavelength has never been observed before. Our analysis finally provides insight into the convergence of the outer GMRES iteration as it shows that the use of deflation results in a tighter clustered spectrum more favorable for the convergence of GMRES [31]. The near-null space components are still insufficiently well resolved as the wavenumber increases to obtain a scalable algorithm. The number of GMRES iterations in the one-dimensional problem considered increases linearly in case the wavenumber is larger than or equal to thousand. We subsequently apply the two-level solver to two-dimensional model problems with constant and nonconstant wavenumber discretized by a second-order finite difference scheme on uniform meshes. Numerical results confirm the result of the theoretical analysis: The convergence of the two-level solver deteriorates for large wavenumber values.

To verify to what extend the aforementioned results carry over to the multilevel method proposed in [1], we present some numerical results for a multilevel extension of the ADEF-1. These results confirm that for small and medium values of the wavenumber, the number of iterations of the multilevel method is constant, but for large wavenumbers, we observe an increase in the number of iterations.

The paper is structured as follows. In Section 2, we describe a Helmholtz problem with and without heterogeneity, its computational domain, and its second-order finite difference discretization. In Section 3, the SLP and multigrid deflation are introduced. Section 4 outlines the multilevel Krylov algorithm. Theoretical results of the Fourier analysis of one-dimensional and two-dimensional Helmholtz problems are presented in Sections 5 and 6, respectively. In Section 7, numerical results supporting the theory are shown, and finally, conclusions are drawn in Section 8.

2. PROBLEM FORMULATION

The Helmholtz equation for the unknown field $u(x, y)$ on a two-dimensional domain Ω with boundary $\partial\Omega$ reads

$$-\Delta u - k^2 u = g \text{ on } \Omega, \tag{2.1}$$

where $k(x, y)$ and $g(x, y)$ are the wavenumber and the source function, respectively. The wavenumber k, the frequency f and angular frequency $\omega = 2\pi f$, the speed of propagation $c(x, y)$, and the wavelength $\lambda = c(x, y)/f$ are related by

DOI: 10.1002/nla

$$k = \frac{2\pi}{\lambda} = \frac{\omega}{c}\,. \tag{2.2}$$

On the boundary $\partial\Omega$, we impose either the homogeneous Dirichlet or the first-order Sommerfeld radiation boundary conditions. By denoting the imaginary unit by ι, the latter is given by

$$\frac{\partial u}{\partial n} - \iota k u = 0 \ \text{ on } \ \partial\Omega\,. \tag{2.3}$$

More accurate radiation conditions are treated in, for example, [13, 22]. We will consider the following two model problems.

Problem 1
In the first problem, we set $\Omega = (0,1) \times (0,1)$, the wavenumber constant, and the source equal to the Dirac delta function

$$g(x,y) = \delta\left(x - \frac{1}{2}, y - \frac{1}{2}\right). \tag{2.4}$$

For the rigorous Fourier analysis, we will consider a one-dimensional variant of this problem.

Problem 2
As the second problem, we consider the so-called wedge-problem introduced in [32] in which $\Omega = (0, 600\,\mathrm{m}) \times (0, 1000\,\mathrm{m})$ is subdivided into three layers in which the wave velocity is set to $c = 2000$ m/s, $c = 1500$ m/s, and $c = 3000$ m/s, respectively. A point source is centered in $x = 300\,\mathrm{m}$ and $y = 0$.

2.1. *Finite difference discretization*

The finite difference discretization of the two aforementioned problems on a uniform mesh with mesh width h in both x and y directions with the stencil

$$[A_h] = \frac{1}{h^2}\begin{bmatrix} 0 & -1 & 0 \\ -1 & 4-\kappa^2 & -1 \\ 0 & -1 & 0 \end{bmatrix} \text{where } \kappa = k\,h \tag{2.5}$$

leads to a system of linear equations

$$A_h x_h = b_h, \tag{2.6}$$

where the discrete Helmholtz operator A_h is complex symmetric and equal to the sum of a stiffness matrix $-\Delta_h$ and $-\kappa^2$ times the identity I_h

$$A_h = -\Delta_h - k^2 I_h\,. \tag{2.7}$$

We discretize the normal derivative on the boundary by using first-order forward differences. We use the rule of thumb that at least 10 nodes per wavelength should be employed, which leads the restriction

$$\kappa \leqslant \frac{2\pi}{10} \approx 0.628\,. \tag{2.8}$$

In some class of problems, the accuracy might require more refined grids, with say 20 or 30 nodes per wavelength. To overcome the pollution error, the expression k^2h^3 should be kept constant, requiring far more points per wavelength for large k [33]. In our experiments, the restriction (2.8) is used, unless mentioned explicitly.

DOI: 10.1002/nla

3. TWO-LEVEL DEFLATED SHIFTED LAPLACE PRECONDITIONER

The linear system matrix A_h in (2.6) is complex-valued, sparse, symmetric, non-Hermitian, and indefinite. The number of eigenvalues with negative real part increases with an increase of the wavenumber k. Solving this linear system on a large scale necessarily requires the use of iterative solution techniques. GMRES [34] and Bi-CGSTAB [35] are suitable choices for this system. Results in [31] show that for the matrices considered in this paper, meaningful bounds on the convergence of GMRES in terms of the eigenvalues of the preconditioned system can be obtained. This motivates the study of how preconditioning and deflation transform the spectrum of the preconditioned matrix such that the resulting system is easier to solve by GMRES. In this work, we make use of the SLP combined with deflation with multigrid vectors. These vectors were constructed geometrically by first standard $h \to H = 2h$ coarsening the fine grid and subsequently setting the columns of the interpolation matrix as deflation vectors. The combination of the preconditioner and the deflation will result in an algorithm referred to as ADEF-1 in the literature [29, 30].

3.1. Shifted Laplace preconditioner

The SLPs are popular preconditioners for the Helmholtz equation. Their development started with the preconditioner obtained by discretizing Laplace operator ($M_h = -\Delta_h$) as proposed in [7]. Later, the Helmholtz operator with an opposite sign in front of the wavenumber ($M_h = -\Delta_h + \kappa^2 I_h$) was considered in [8]. Subsequently, a Laplace operator with a complex shift was introduced in [10, 36] and found to be more effective. Denoting by β_1 and β_2 two real numbers, the complex SLP can be written as

$$M_{h,(\beta_1,\beta_2)} = -\Delta_h - (\beta_1 - \imath\beta_2)\kappa^2 I_h, \quad \beta_1, \beta_2 \in \mathbb{R}\,, \tag{3.1}$$

and the preconditioned operator as

$$S_{h,(\beta_1,\beta_2)} = M^{-1}_{h,(\beta_1,\beta_2)} A_h\,. \tag{3.2}$$

The complex shift introduces damping and renders the preconditioned system amenable to approximate inversion using either geometric multigrid [1, 36] or MILU [9]. More recently, algebraic multigrid has been used to invert the preconditioner [14, 15].

The spectral properties of the shifted Laplace preconditioned Helmholtz operator $M^{-1}_{h,(\beta_1,\beta_2)} A_h$ are elaborated in [26]. This paper shows that the introduction of damping renders the problem easier to solve and that the spectrum consists of a cluster in the complex plane near one and some eigenvalues that lie at a distance of $O(\epsilon/k^2)$ from the origin where ϵ is a small number not depending upon k. As k increases, the smallest eigenvalues go to zero causing the convergence of the outer Krylov subspace iteration to slow down. For fixed k, the number of iterations remains constant as the mesh width h is reduced. A reduction of the number of iterations has not been observed. The paper [26] also shows that the difficulty in solving the problem with Dirichlet boundary conditions is representative for problems with radiation boundary conditions. In this paper, we analyze how the use of deflation with multigrid vectors affects the convergence.

3.2. Two-level deflation

Multigrid vectors affect the convergence. Deflation is a technique to deal with small eigenvalues in the preconditioned system that adversely affect the convergence of a Krylov subspace iteration [29, 30]. The basic idea is to bring the small eigenvalues to zero by a projection procedure. Denoting the size of A_h by n, we define the matrix $Z_h \in \mathbb{R}^{n\times r}$ whose $r < n$ columns are the deflation vectors. These vectors should be chosen such that the matrix Z_h has full rank. Then, the Galerkin or coarse-level matrix becomes $E_h = Z_h^T A_h Z_h$. Given Z_h, we define the deflation operator $P_h \in \mathbb{C}^{n\times n}$ as

$$P_h = I_h - A_h Q_h \text{ where } Q_h = Z_h E_h^{-1} Z_h^T \text{ and } E_h = Z_h^T A_h Z_h\,. \tag{3.3}$$

Observe that Q_h inherits the complex symmetry from A_h. As P_h is a projection, its spectrum consists of 0 and 1.

DOI: 10.1002/nla

In this paper, we will perform deflation with geometrically constructed multigrid vectors. We therefore assume that p is a nonzero natural number and discretize Ω by a uniform mesh with $n = 2^p$ elements and mesh width $h = 1/n$ in each direction. Standard $h \to H = 2h$ coarsening of the fine mesh Ω^h will result in a coarse mesh Ω^H. As a prolongation operator, we choose the bilinear interpolation operator such that fine grid points not belonging to the coarse grid have the stencil

$$\left[I_H^h\right] = \frac{1}{4}\begin{bmatrix} 1 & 2 & 1 \\ 2 & 4 & 2 \\ 1 & 2 & 1 \end{bmatrix}_H^h . \tag{3.4}$$

To satisfy the requirement on the restriction I_h^H that $I_h^H = c\left(I_H^h\right)^T$ with c as a constant scalar, we choose a full-weighting restriction operator. Corresponding equivalents for one-dimensional problems are used. We set the matrix Z_h in (3.3) equal to the coarse-to-fine grid interpolation operator I_H^h. With this choice, the deflation operator $P_{h,H}$ defined by (3.3) coincides with the transpose of the two-grid correction operator with a coarse-grid operator A_H build by Galerkin coarsening, that is,

$$P_{h,H} = I_h - A_h\, Q_{h,H} \text{ where } Q_{h,H} = I_H^h A_H^{-1} I_h^H \text{ and } A_H = I_h^H A_h I_H^h, \tag{3.5}$$

whereas both A_h and $Q_{h,H}$ are complex symmetric

$$P_{h,H}^T = I_h - Q_{h,H} A_h . \tag{3.6}$$

The deflation here described shifts troublesome eigenvalues to the origin unlike multigrid methods that push such eigenvalues to unity. For large problems, the exact inversion of A_H is impractical, and one has to resort to approximate solvers instead. Without proper care, this will however lead to the introduction of close-to-zero eigenvalues in the preconditioned systems. This can be avoided by controlling the approximate solver with A_H or by deflating to the largest eigenvalue of the preconditioned system. These issues are further discussed in the multilevel extension of the algorithm in Section 4.

3.3. Two-level preconditioner

Applying the SLP preconditioner (3.2) to the multilevel deflated system requires solving a system with $M_{h,(\beta_1,\beta_2)}^{-1} P_{h,H} A_h$ as coefficient matrix. Applying the multilevel deflation operator (3.6) to the SLP preconditioned system instead leads to a system with $P_{h,H}^T M_{h,(\beta_1,\beta_2)}^{-1} A_h$ as coefficient matrix. The rigorous Fourier analysis in the sequel of this paper shows that in the case of homogeneous Dirichlet boundary conditions, and in the case that both the SLP preconditioner $M_{h,(\beta_1,\beta_2)}$ and the coarse-grid operator A_H are inverted exactly, a basis of discrete sine modes exists that allows to diagonalize both A_h and $M_{h,(\beta_1,\beta_2)}$ and to block-diagonalize $P_{h,H}$. This immediately implies that the two aforementioned coefficient matrices have the same spectrum, that is,

$$\sigma\left(M_{h,(\beta_1,\beta_2)}^{-1} P_{h,H} A_h\right) = \sigma\left(P_{h,H}^T M_{h,(\beta_1,\beta_2)}^{-1} A_h\right). \tag{3.7}$$

A more general proof of this identify is given in [30]. The presence of roundoff errors however gives rise to algorithms referred to in the literature as ADEF-1 and ADEF-2, respectively [29, 30]. Whereas we implemented ADEF-2 according to the scheme shown in Figure 1 to generate the numerical results in Section 7, we study ADEF-1 in our Fourier analysis. In this analysis, we will denote the deflated preconditioned operator as

$$B_{h,H,(\beta_1,\beta_2)} = P_{h,H}^T M_{h,(\beta_1,\beta_2)}^{-1} A_h = P_{h,H}^T S_{h,(\beta_1,\beta_2)} \tag{3.8}$$

DOI: 10.1002/nla

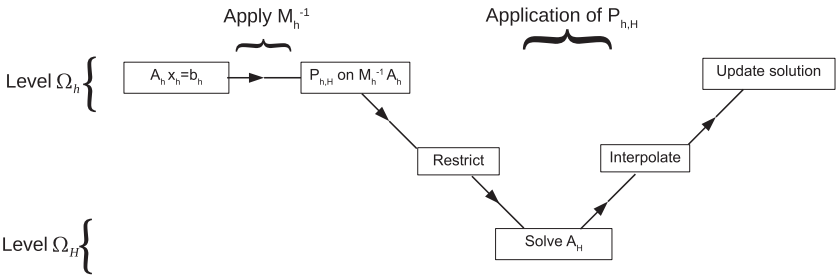

Figure 1. A schematic representation of the two-level ADEF-2 algorithm considered.

and use the following notation

$$\text{diag}\begin{bmatrix} d_1 \\ d_2 \end{bmatrix} = \begin{bmatrix} d_1 & 0 \\ 0 & d_2 \end{bmatrix}$$

and

$$\text{diag}\begin{bmatrix} d_1 \\ d_2 \\ d_3 \\ d_4 \end{bmatrix} = \begin{bmatrix} d_1 & 0 & 0 & 0 \\ 0 & d_2 & 0 & 0 \\ 0 & 0 & d_3 & 0 \\ 0 & 0 & 0 & d_4 \end{bmatrix}.$$

4. MULTILEVEL KRYLOV METHOD

The algorithm described in the previous section can be viewed as a two-level preconditioner for an outer Krylov iteration in which the SLP preconditioner (3.1) acting on the first level is combined with the multigrid deflation algorithm (3.5) acting on the second. The SLP preconditioner can be approximated by using standard multigrid cycle [12]. The multigrid deflation requires the solution of a coarse-grid problem with A_H as coefficient matrix. As this matrix has the same properties of the original operator, the preconditioned Krylov method just described can be applied recursively on the condition that a flexible outer subspace Krylov method such as GCR [37] is employed. This approach gives rise to a multilevel algorithm. Note however that convergence of the outer Krylov method critically depends on the accuracy to which the system with A_H as coefficient matrix is solved. Indeed, an approximate coarse grid solver will yield a deflated operator with near-zero eigenvalues slowing down the convergence. The deflation operator is therefore adapted in such a way that the undesired eigenvalues are shifted to the largest eigenvalue, which in case of the SLP preconditioned Helmholtz is one, instead of zero. The multilevel algorithm in which a V-cycle is used to approximate the SLP preconditioner is named ML-ADEF-1. Numerical results with ML-ADEF-1 as a preconditioner for GCR acceleration will be presented in Section 7.5.

5. ONE-DIMENSIONAL TWO-GRID FOURIER ANALYSIS

In this section, we perform a rigorous two-grid Fourier analysis of the solver proposed earlier in a one-dimensional setting. We therefore consider the Helmholtz equation (2.1) supplied with homogeneous Dirichlet boundary conditions discretized on $\Omega = (0,\ 1)$. Dirichlet boundary conditions are easy to analyze. Furthermore, as these boundary conditions do not introduce any damping, the analysis that follows can be considered to be a worst-case analysis for the problem with Sommerfeld boundary conditions. This fact will be illustrated by numerical results in Section 7.3. The discretization of the Helmholtz equation on a uniform mesh $\Omega^h \subset (0, 1)$ with mesh width $h = 1/n$ using the second-order accurate stencil

$$[A_h] = \frac{1}{h^2}\begin{bmatrix} -1 & 2-\kappa^2 & -1 \end{bmatrix} \text{ where } \kappa = k\,h\,, \tag{5.1}$$

DOI: 10.1002/nla

results after elimination of the boundary conditions in the linear system

$$A_h x_h = b_h\,, \tag{5.2}$$

where $A_h \in \mathbb{C}^{(n-1)\times(n-1)}$. Given the preconditioner $M_{h,(\beta_1,\beta_2)}$ defined in (3.1) and the multigrid deflation operator $P_{h,H}$ defined in (3.5), the goal of our analysis is to find all eigenvalues of the deflated preconditioned operator $B_{h,H,(\beta_1,\beta_2)}$. In this analysis, we assume that both the preconditioner $M_{h,(\beta_1,\beta_2)}$ and the coarse grid matrix A_H are inverted exactly. Details of our analysis can be found in our technical report [38] and the monograph [39].

We denote by $\underline{x} \in \mathbb{R}^{n-1}$ the vector with components $x_i = i\,h$ and start our analysis by observing that the grid vectors $\phi_h^\ell \in \mathbb{R}^{n-1}$ for $1 \leqslant \ell \leqslant n-1$ with components

$$\phi_{h,i}^\ell = \sin(\ell\pi x_i) \tag{5.3}$$

are eigenvectors of A_h corresponding to the eigenvalues

$$\lambda^\ell(A_h) = \frac{1}{h^2}\left(2 - 2\mathrm{c}_\ell - \kappa^2\right)\,, \tag{5.4}$$

where $c_\ell = \cos(\ell\pi h)$. This implies that the same grid vectors are eigenvectors of the preconditioner $M_{h,(\beta_1,\beta_2)}$ and of the preconditioned operator (or smoother) $S_{h,(\beta_1,\beta_2)}$ corresponding to the eigenvalues

$$\lambda^\ell(M_{h,(\beta_1,\beta_2)}) = \frac{1}{h^2}\left(2 - 2\mathrm{c}_\ell - \kappa^2(\beta_1 - \imath\beta_2)\right)\,, \tag{5.5}$$

and

$$\lambda^\ell(S_{h,(\beta_1,\beta_2)}) = \frac{2 - 2\mathrm{c}_\ell - \kappa^2}{2 - 2\mathrm{c}_\ell - \kappa^2(\beta_1 - \imath\beta_2)}\,, \tag{5.6}$$

respectively.

The multigrid deflation (or coarse grid correction) operator $P_{h,H}^T$ employs a coarser grid with mesh width $H = 2h$ and as intergrid transfer and coarser operators the one-dimensional variants of those described above. By reordering the eigenvectors of A_h in a standard way in $(\ell, n-\ell)$ harmonics, we obtain the basis

$$V_h = \left\{\left(\phi_h^\ell, \phi_h^{n-\ell}\right) \mid \ell = 1,\ldots,n/2-1\right\} \cup \left\{\phi_h^{n/2}\right\} \tag{5.7}$$

in which $P_{h,H}^T$ can be written in a block-diagonal form; that is, we can write

$$P_{h,H}^T = \left[\left(P_{h,H}^\ell\right)^T\right]_{1\leqslant\ell\leqslant n/2}\,, \tag{5.8}$$

where the individual blocks are given by

$$P_{h,H}^\ell = I - \left(I_H^h\right)^\ell \left(A_H^\ell\right)^{-1} \left(I_h^H\right)^\ell A_h^\ell\,. \tag{5.9}$$

A standard computation gives the 2×1 blocks of the bilinear interpolation where for $1 \leqslant \ell \leqslant n/2-1$,

$$\left(I_H^h\right)^\ell = \frac{1}{2}\begin{bmatrix} (1+c_\ell) \\ -(1-c_\ell) \end{bmatrix}\,, \tag{5.10}$$

and where

$$\left(I_H^h\right)^{n/2} = 0\,. \tag{5.11}$$

DOI: 10.1002/nla

The Galerkin coarsening then results in the 1×1 blocks where for $1 \leqslant \ell \leqslant n/2 - 1$,

$$A_H^\ell = \left(I_h^H\right)^\ell A_h^\ell \left(I_H^h\right)^\ell = \frac{1}{2h^2}\left[2\left(1 - c_\ell^2\right) - \kappa^2\left(1 + c_\ell^2\right)\right] \tag{5.12}$$

and where

$$A_H^{n/2} = 0\,. \tag{5.13}$$

A straightforward computation subsequently allows to obtain, for $1 \leqslant \ell \leqslant n/2 - 1$, the following 2×2 blocks of $\left(P_{h,H}^\ell\right)^T$

$$\left(P_{h,H}^\ell\right)^T = \frac{1}{\text{Ç}}\begin{bmatrix} -(\mathrm{c}_\ell + 1)\left(\mathrm{c}_\ell^2 - 1\right) + \frac{1}{2}\kappa^2\left(\mathrm{c}_{\ell_2}^2 - 1\right) & \frac{1}{2}\left(\mathrm{c}_\ell^2 - 1\right)\left(2 + 2\mathrm{c}_\ell - \kappa^2\right) \\ \frac{1}{2}\left(\mathrm{c}_\ell^2 - 1\right)\left(-2 + 2\mathrm{c}_\ell + \kappa^2\right) & \left(\mathrm{c}_\ell^2 - 1\right)(3 + \mathrm{c}_\ell) + \frac{1}{2}\kappa^2\left(\mathrm{c}_\ell^2 + 3\right) \end{bmatrix}$$

where $\text{Ç} = 2\left(1 - \mathrm{c}_\ell^2\right) + \kappa^2\left(\mathrm{c}_\ell^2 + 1\right)$, and the 1×1 block

$$\left(P_{h,H}^{n/2}\right)^T = 1\,. \tag{5.14}$$

The basis V_h (5.7) can therefore be used to block-diagonalize the deflated preconditioned operator; that is, we can write

$$B_{h,H,(\beta_1,\beta_2)} = \left[B_{h,H,(\beta_1,\beta_2)}^\ell\right]_{1 \leqslant \ell \leqslant n/2} \tag{5.15}$$

where for $1 \leqslant \ell \leqslant n/2 - 1$, $B_{h,H,(\beta_1,\beta_2)}^\ell$ is the 2×2 matrix

$$B_{h,H,(\beta_1,\beta_2)}^\ell = \left(P_{h,H}^\ell\right)^T \operatorname{diag}\begin{bmatrix} \lambda^\ell\left(S_{h,(\beta_1,\beta_2)}\right) \\ \lambda^{n-\ell}\left(S_{h,(\beta_1,\beta_2)}\right) \end{bmatrix} \tag{5.16}$$

and where

$$B_{h,H,(\beta_1,\beta_2)}^{n/2} = \lambda^{n/2}\left(S_{h,(\beta_1,\beta_2)}\right) = \frac{2 - \kappa^2}{2 - \kappa^2(\beta_1 - \imath\beta_2)}\,. \tag{5.17}$$

This block-diagonal form renders an analytical computation of the eigenvalues of $B_{h,H,(\beta_1,\beta_2)}$ feasible and results in the conclusion that $B_{h,H,(\beta_1,\beta_2)}$ has a zero eigenvalue of multiplicity $n/2-1$, the eigenvalue (5.17), and $n/2 - 1$ eigenvalues of the form

$$\lambda^\ell(B_{h,H,(\beta_1,\beta_2)}) = \frac{a_\ell + \imath b_\ell}{c_\ell + \imath d_\ell} \text{ for } 1 \leqslant \ell \leqslant n/2 - 1, \tag{5.18}$$

where a_ℓ, b_ℓ, c_ℓ, and d_ℓ are third-order polynomials in κ^2 and given by

$$\begin{aligned}
a_\ell &= \left(-1 - \mathrm{c}_\ell{}^2\right)\beta_1\kappa^6 + \left(4\beta_1 + 2 - 2\mathrm{c}_\ell{}^2 + 4\mathrm{c}_\ell{}^2\beta_1\right)\kappa^4 \\
&\quad + \left(8\mathrm{c}_\ell{}^2 - 4\beta_1 - 8 + 4\mathrm{c}_\ell{}^4\beta_1\right)\kappa^2 + \left(8 - 16\mathrm{c}_\ell{}^2 + 8\mathrm{c}_\ell{}^4\right) \\
b_\ell &= \left(1 + \mathrm{c}_\ell{}^2\right)\beta_2\kappa^6 + \left(-4\mathrm{c}_\ell{}^2\beta_2 - 4\beta_2\right)\kappa^4 + \left(4\beta_2 - 4\mathrm{c}_\ell{}^4\beta_2\right)\kappa^2 \\
c_\ell &= \left(\beta_2{}^2 - \beta_1{}^2 + \mathrm{c}_\ell{}^2\beta_2{}^2 - \mathrm{c}_\ell{}^2\beta_1{}^2\right)\kappa^6 \\
&\quad + \left(4\beta_1 - 2\mathrm{c}_\ell{}^2\beta_1{}^2 + 2\mathrm{c}_\ell{}^2\beta_2{}^2 + 2\beta_1{}^2 - 2\beta_2{}^2 + 4\mathrm{c}_\ell{}^2\beta_1\right)\kappa^4 \\
&\quad + \left(8\beta_1\mathrm{c}_\ell{}^2 - 8\beta_1 - 4 + 4\mathrm{c}_\ell{}^4\right)\kappa^2 + 8\mathrm{c}_\ell{}^4 + 8 - 16\mathrm{c}_\ell{}^2 \\
d_\ell &= \left(2\beta_1\beta_2 + 2\mathrm{c}_\ell{}^2\beta_1\beta_2\right)\kappa^6 + \left(4\mathrm{c}_\ell{}^2\beta_1\beta_2 - 4\beta_1\beta_2 - 4\beta_2 - 4\mathrm{c}_\ell{}^2\beta_2\right)\kappa^4 \\
&\quad + \left(8\beta_2 - 8\mathrm{c}_\ell{}^2\beta_2\right)\kappa^2.
\end{aligned}$$

DOI: 10.1002/nla

In the remainder of this section, we will use the aforementioned expression to investigate the behavior of the spectrum of $B_{h,H,(\beta_1,\beta_2)}$ in three parameter studies: varying wavenumber, varying the number of grid points per wavelength, and varying the imaginary part in the shift β_2. In Figures 2–4, we plot the spectrum studied in the complex plane. We observe that the zero eigenvalue of $B_{h,H,(\beta_1,\beta_2)}$ does not influence the convergence of the outer Krylov subspace acceleration and is therefore left out of our considerations.

Figure 2 shows the nonzero part of the spectrum of $B_{h,H,(\beta_1=1,\beta_2=1)}$ for $k = 100$, $k = 1000$, and $k = 10,000$ using 20 grid points per wavelength (and thus $\kappa = 0.3215$). The magnitude of the smallest eigenvalue in size is explicitly given. This figure shows that the spectrum for $k = 100$

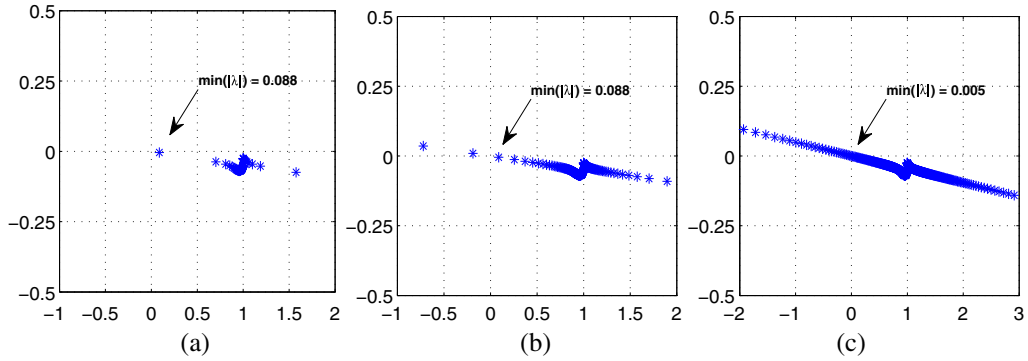

Figure 2. Nonzero part of $\sigma(B_{h,H,(1,\ 1)})$ in the one-dimensional problem for various wavenumbers k satisfying $\kappa = 0.3215$. (a) $k = 100$, (b) $k = 1000$, and (c) $k = 10,000$.

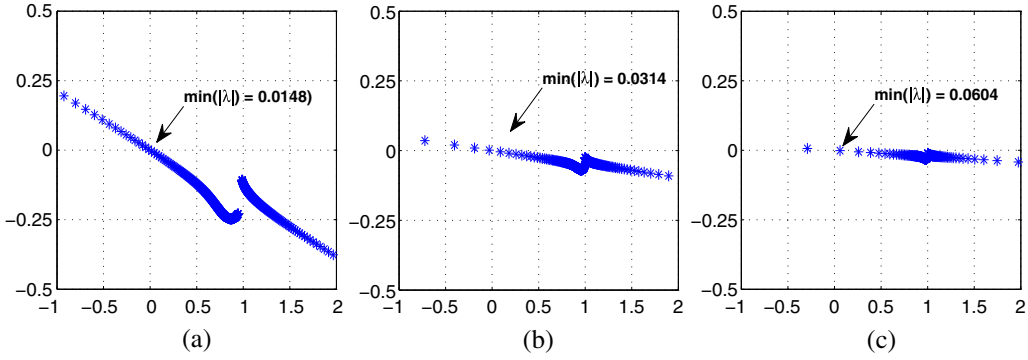

Figure 3. Nonzero part of $\sigma(B_{h,H,(1,\ 1)})$ in the one-dimensional problem for $\kappa = 2000$ and for various values of κ. (a) $\kappa = 0.625$,(b) $\kappa = 0.3215$, and (c) $\kappa = 0.2015$.

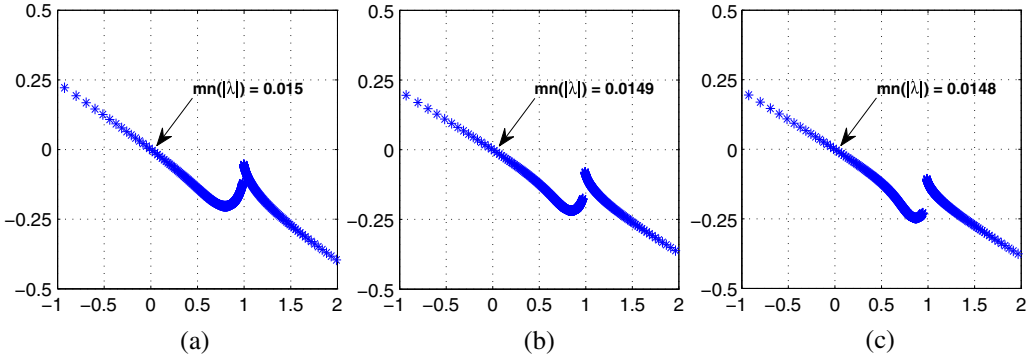

Figure 4. Nonzero part of $\sigma(B_{h,H,(1,\ \beta_2)})$ in the one-dimensional problem for $k = 2000$ and for various values of β_2 satisfying $\kappa = 0.625$. (a) $\beta_2 = 0.5$, (b) $\beta_2 = 0.75$, and (c) $\beta_2 = 1$.

DOI: 10.1002/nla

is clustered around $(0.5, 0)$ on the complex plane. As the wavenumber increases, however, the spectrum smears out on both sides, and eigenvalues shift toward the origin. Eigenvalues with a negative real part appear. In the range of wavenumbers considered, the smallest eigenvalue decreases by more than one order of magnitude. On the basis of these observations, we expect GMRES to converge fast for k up to 100. For larger wavenumbers, however, the increasing number of small eigenvalues prevents the solver from being scalable. This nonscalability becomes even more pronounced in two dimensions as will be confirmed by further analysis and numerical experiments.

Figure 3 shows the nonzero spectrum of $B_{h,H,(\beta_1=1,\beta_2=1)}$ for $k = 2000$ and for $\kappa = 0.625$, $\kappa = 0.312$, and $\kappa = 0.2015$. The magnitude of the smallest eigenvalue is again shown. This figure shows that the number of small eigenvalues decreases, that the spectrum becomes more clustered, and the deflated preconditioned system becomes easier to solve by Krylov subspace methods as the number of grid points per wavelength is increased. This effect has not been observed when the SLP preconditioner is used without deflation.

Figure 4 shows the nonzero spectrum of $B_{h,H,(\beta_1=1,\beta_2)}$ for $\kappa = 0.625$, for $k = 2000$, and for $\beta_2 = 0.5$, $\beta_2 = 0.75$, and $\beta_2 = 1$. This figure shows that, contrary to the case in which the SLP preconditioner is used without deflation, the spectrum remains virtually unchanged as β_2 increases. The SLP preconditioner becomes more diagonally dominant as β_2 increases. This result opens promising perspectives to obtain a good approximation of the preconditioner at low cost.

Figure 5 finally shows a bar plot of the modulus $|\lambda^\ell|$ of the eigenvalues of $B_{h,H,(\beta_1=1,\beta_2=1)}$ in magnitude close to zero for $\kappa = 0.625$ and $\kappa = 0.3215$ and for various values for k. The numbering ℓ in this figure corresponds to the one defined earlier. This figure clearly shows that the number of small eigenvalues grows with k and that this effect is more pronounced in case a smaller number of grid points per wavelength is used (which corresponds to a larger value of κ). This figure therefore confirms the findings discussed earlier for Figure 3.

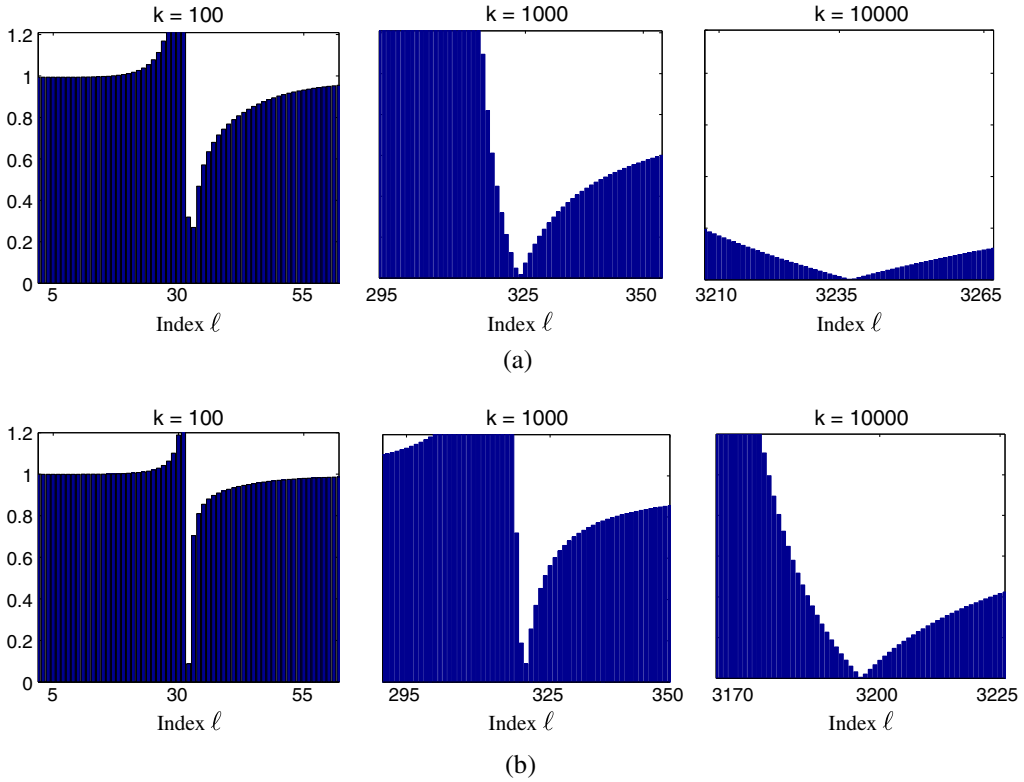

Figure 5. Magnitude $|\lambda|$ of nonzero part of $\lambda \in \sigma(B_{h,H,(1,1)})$ in the one-dimensional problem for $\kappa = 0.625$ and $\kappa = 0.3215$ and various values of k. The eigenvalues are ordered according to the index ℓ defined in the Fourier analysis. (a) $\kappa = 0.625$ and (b) $\kappa = 0.3215$.

DOI: 10.1002/nla

6. TWO-DIMENSIONAL TWO-GRID FOURIER ANALYSIS

In this section, we extend the analysis of the previous section to two dimensions. We therefore consider the Helmholtz equation (2.1) supplied with homogeneous Dirichlet boundary conditions discretized on $\Omega = (0,1)\times(0,1)$. As before, we assume the preconditioner $M_{h,(\beta_1,\beta_2)}$ and the coarse grid operator A_H to be inverted exactly. The second-order finite difference discretization using the stencil (2.5) results after elimination of the boundary conditions in the linear system

$$A_h x_h = b_h \tag{6.1}$$

where $A_h \in \mathbb{C}^{(n-1)^2\times(n-1)^2}$.

We denote by $\underline{x}, \underline{y} \in \mathbb{R}^{n-1}$ the vectors with components $x_i = i\,h$ and $y_i = i\,h$ and observe that the grid vectors $\phi_h^{\ell_1,\ell_2} \in \mathbb{R}^{(n-1)^2}$ for $1 \leqslant \ell_1, \ell_2 \leqslant n-1$ with components

$$\phi_{h,j(n-1)+i}^{\ell_1,\ell_2} = \sin(\ell_1 \pi x_i)\sin(\ell_2 \pi y_j) \tag{6.2}$$

are eigenvectors of A_h corresponding to the eigenvalues

$$\lambda^{\ell_1,\ell_2}(A_h) = \frac{1}{h^2}\left(4 - 2\mathrm{c}_{\ell_1} - 2\mathrm{c}_{\ell_2} - \kappa^2\right), \tag{6.3}$$

where $\mathrm{c}_{\ell_1} = \cos(\ell_1 \pi h)$ and $\mathrm{c}_{\ell_2} = \cos(\ell_2 \pi h)$. The eigenvalues of the preconditioner $M_{h,(\beta_1,\beta_2)}$ and the preconditioned operator $S_{h,(\beta_1,\beta_2)} = M_{h,(\beta_1,\beta_2)}^{-1} A_h$ are therefore given by

$$\lambda^{\ell_1,\ell_2}\left(M_{h,(\beta_1,\beta_2)}\right) = \frac{1}{h^2}\left[4 - 2\mathrm{c}_{\ell_1} - 2\mathrm{c}_{\ell_2} - (\beta_1 - \iota\beta_2)\kappa^2\right] \tag{6.4}$$

and

$$\lambda^{\ell_1,\ell_2}\left(S_{h,(\beta_1,\beta_2)}\right) = \frac{4 - 2\mathrm{c}_{\ell_1} - 2\mathrm{c}_{\ell_2} - \kappa^2}{4 - 2\mathrm{c}_{\ell_1} - 2\mathrm{c}_{\ell_2} - \kappa^2(\beta_1 - \iota\beta_2)}, \tag{6.5}$$

respectively.

To block-diagonalize the multigrid deflation operator $P_{h,H}^T$, we again reorder the basis of eigenvectors of A_h in a standard way in
$((\ell_1,\ell_2),(n-\ell_1,n-\ell_2),(\ell_1,n-\ell_2),(n-\ell_1,\ell_2))$ harmonics [39] to obtain the basis

$$\begin{aligned} V_h = &\left\{\left(\phi_h^{\ell_1,\ell_2}, \phi_h^{n-\ell_1,n-\ell_2}, \phi_h^{\ell_1,n-\ell_2}, \phi_h^{\ell_1,n-\ell_2}\right) \mid \ell_1,\ell_2 = 1,\ldots,n/2-1\right\} \\ &\cup \left\{\left(\phi_h^{\ell_1,n/2}, \phi_h^{n-\ell_1,n/2}\right) \mid \ell_1 = 1,\ldots,n/2-1\right\} \\ &\cup \left\{\left(\phi_h^{n/2,\ell_2}, \phi_h^{n/2,n-\ell_2}\right) \mid \ell_2 = 1,\ldots,n/2-1\right\} \cup \left\{\phi_h^{n/2,n/2}\right\}. \end{aligned} \tag{6.6}$$

In this basis, $P_{h,H}^T$ can be written in a block diagonal form; that is, we can write

$$P_{h,H}^T = \left[\left(P_{h,H}^{\ell_1,\ell_2}\right)^T\right]_{1\leqslant\ell_1,\ell_2\leqslant n/2}, \tag{6.7}$$

where the individual blocks are given by

$$\left(P_{h,H}^{\ell_1,\ell_2}\right)^T = I - \left(I_H^h\right)^{\ell_1,\ell_2}\left(A_H^{\ell_1,\ell_2}\right)^{-1}\left(I_h^H\right)^{\ell_1,\ell_2} A_h^{\ell_1,\ell_2}. \tag{6.8}$$

A standard computation results in the 4×1 blocks of the bilinear interpolation I_H^h where for $1 \leqslant \ell_1, \ell_2 \leqslant n/2-1$,

$$\left(I_H^h\right)^{\ell_1,\ell_2} = \frac{1}{4}\begin{bmatrix} \left(1+\mathrm{c}_{\ell_1}\right)\left(1+\mathrm{c}_{\ell_2}\right) \\ \left(1-\mathrm{c}_{\ell_1}\right)\left(1-\mathrm{c}_{\ell_2}\right) \\ \left(1+\mathrm{c}_{\ell_1}\right)\left(1-\mathrm{c}_{\ell_2}\right) \\ \left(1-\mathrm{c}_{\ell_1}\right)\left(1+\mathrm{c}_{\ell_2}\right) \end{bmatrix} \tag{6.9}$$

DOI: 10.1002/nla

and where for other values of ℓ_1 and ℓ_2,

$$\left(I_H^h\right)^{\ell 1,\ell_2} = 0\,. \tag{6.10}$$

The Galerkin coarsening gives the 1×1 blocks where for $1 \leqslant \ell_1, \ell_2 \leqslant n/2 - 1$,

$$\begin{aligned} A_H^{\ell_1,\ell_2} = \frac{1}{h^2}\Big[4\left(1 - 2\,\mathrm{c}_{\ell_1}\mathrm{c}_{\ell_2} + \mathrm{c}_{\ell_1}^2 + \mathrm{c}_{\ell_2}^2 + \mathrm{c}_{\ell_1}^2\mathrm{c}_{\ell_2}^2 - \mathrm{c}_{\ell_1}^3\mathrm{c}_{\ell_2} - \mathrm{c}_{\ell_1}\mathrm{c}_{\ell_2}^3\right) \\ -\kappa^2\left(1 + \mathrm{c}_{\ell_1}^2 + \mathrm{c}_{\ell_2}^2 + \mathrm{c}_{\ell_1}^2\mathrm{c}_{\ell_2}^2\right)\Big] \end{aligned} \tag{6.11}$$

and where for other values of ℓ_1 and ℓ_2,

$$A_H^{\ell_1,\ell_2} = 0\,. \tag{6.12}$$

The 4×4 blocks of the multigrid deflation operator $P_{h,H}^T$ can subsequently be computed for $1 \leqslant \ell_1, \ell_2 \leqslant n/2 - 1$. For other values of ℓ_1 and ℓ_2, these blocks are of size either 2×2 or 1×1 and equal to the identity.

The basis V_h (6.6) can therefore be used to block-diagonalize the deflated preconditioned operator; that is, we can write

$$B_{h,H,(\beta_1,\beta_2)} = \left[B_{h,H,(\beta_1,\beta_2)}^{\ell_1,\ell_2}\right]_{1\leqslant\ell_1,\ell_2\leqslant n/2} \tag{6.13}$$

where for $1 \leqslant \ell_1, \ell_2 \leqslant n/2 - 1$, $B_{h,H,(\beta_1,\beta_2)}^{\ell}$ is the 4×4 block

$$B_{h,H,(\beta_1,\beta_2)}^{\ell_1,\ell_2} = \left(P_{h,H}^{\ell_1,\ell_2}\right)^T \ \mathrm{diag}\begin{bmatrix} \lambda^{\ell_1,\ell_2}\left(S_{h,(\beta_1,\beta_2)}\right) \\ \lambda^{n-\ell_1,n-\ell_2}\left(S_{h,(\beta_1,\beta_2)}\right) \\ \lambda^{n-\ell_1,\ell_2}\left(S_{h,(\beta_1,\beta_2)}\right) \\ \lambda^{\ell_1,n-\ell_2}\left(S_{h,(\beta_1,\beta_2)}\right) \end{bmatrix}, \tag{6.14}$$

and where for other values of ℓ_1 and ℓ_2, $B_{h,H,(\beta_1,\beta_2)}^{\ell_1,\ell_2}$ is either a 2×2 block, for example,

$$B_{h,H,(\beta_1,\beta_2)}^{\ell_1,n/2} = \mathrm{diag}\begin{bmatrix} \lambda^{\ell_1,n/2}\left(S_{h,(\beta_1,\beta_2)}\right) \\ \lambda^{n-\ell_1,n/2}\left(S_{h,(\beta_1,\beta_2)}\right) \end{bmatrix} \tag{6.15}$$

or the 1×1 block

$$B_{h,H,(\beta_1,\beta_2)}^{n/2,n/2} = \lambda^{n/2,n/2}\left(S_{h,(\beta_1,\beta_2)}\right) = \frac{4-\kappa^2}{4-\kappa^2(\beta_1 - \iota\beta_2)}\,. \tag{6.16}$$

The eigenvalues of $B_{h,H,(\beta_1,\beta_2)}$ can therefore be computed numerically as the eigenvalues of the separate blocks. In the remainder of this section, we will present the results of such computations that confirm the properties of the solver revealed in the previous section.

Figure 6 shows the nonzero part of the spectrum of $B_{h,H,(\beta_1=1,\beta_2=1)}$ for $k = 30$, $k = 60$, and $k = 120$ using 10 grid points per wavelength (and thus $\kappa = 0.625$). The value of the eigenvalue smallest in size is given. For $k = 30$, the spectrum is clustered away from the origin. As the wavenumbers increase, the radius of the cluster increases. Eigenvalues close to the origin and eigenvalues with a negative real part appear. The number of unresolved near-null space eigenmodes grows substantially faster than in the one-dimensional case. These unresolved modes hamper the solver from being scalable.

Figure 7 shows the magnitude of the five eigenvalues smallest in size of $\sigma(B_{h,H,(1,\,1)})$ versus the wavenumber for $\kappa = 0.625$ (left) and $\kappa = 0.3215$ (right) on a logarithmic scale. This figure serves to further illustrate the observation made earlier for Figure 6 that the eigenvalues shift to the origin as the wavenumber increases and that this effect is more pronounced in case that a small number of grid points per wavelength is used.

DOI: 10.1002/nla

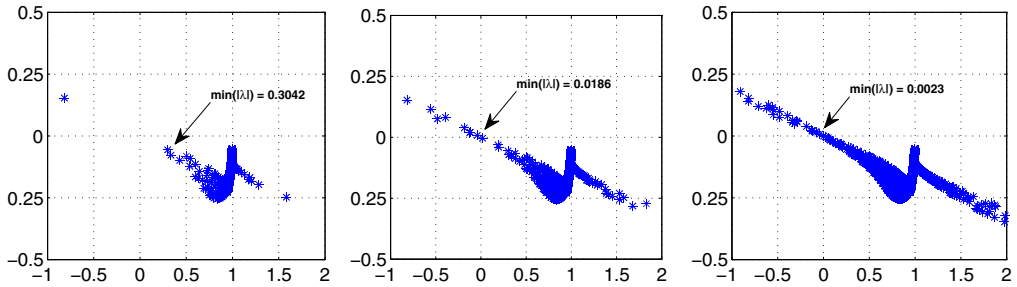

Figure 6. Nonzero part of $\sigma(B_{h,H,(1,\,1)})$ for the two-dimensional problem for various values of k satisfying $\kappa = 0.625$. (a) $k = 30$, (b) $k = 60$, and (c) $k = 120$.

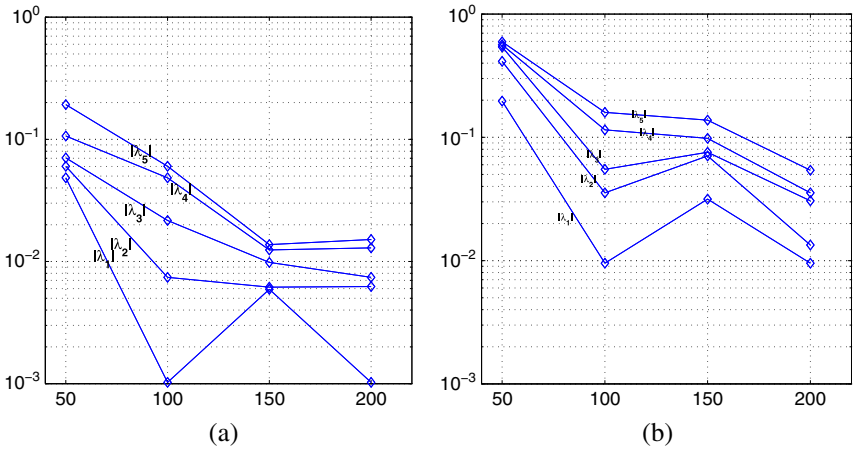

Figure 7. Magnitude of the five eigenvalues smallest in size of $\sigma(B_{h,H,(1,\,1)})$ versus the wavenumber in the two-dimensional problem for (a) $\kappa = 0.625$ and (b) $\kappa = 0.3215$.

7. NUMERICAL EXPERIMENTS

In this section, we perform numerical experiments on the constant (Problem 1) and nonconstant (Problem 2) wavenumber problems described in Section 2 aiming at various goals. First, in Section 7.1, we show that using deflation allows us to make the SLP preconditioner more diagonally dominant by increasing the imaginary part in the shift (β_2) without paying any penalty in the number of GMRES iterations. Next, in Section 7.2, we employ the one-dimensional problem with Sommerfeld boundary conditions to show that the number of deflated preconditioned GMRES iterations remains constant up to $k = 800$ and grows linearly starting at $k = 1000$. Subsequently, in Section 7.3, we show how imposing Dirichlet boundary conditions in our Fourier analysis can be justified and how the use of deflation affects the number of preconditioned GMRES iterations. We repeat these experiments for the nonconstant wavenumber problem in Section 7.4. Until here, we employ a two-level version of our algorithm. Finally, in Section 7.5, we conduct numerical experiments with the multilevel extension of the algorithm to give further evidence of the nonscalability of the algorithm at sufficiently high wavenumbers. In our experiments, we use a zero starting guess and stop the outer Krylov subspace iterations if

$$\frac{\|b_h - A_h x\|_2}{\|b_h\|_2} \leqslant 10^{-7}\,. \tag{7.1}$$

DOI: 10.1002/nla

7.1. *Influence of the imaginary part of the shift*

In Figure 8, we plotted the required number of GMRES iterations to solve Problems 1 and 2 with first-order Sommerfeld boundary conditions as a function of the imaginary shift β_2. In Problems 1 and 2, we used $k = 50$ and $f = 30$, respectively, and employed 10 grid points per wavelength. We have chosen $\beta_1 = 1$ and allowed β_2 to vary between 0 and 1. For $\beta_2 = 0$, the SLP preconditioner coincides with the discrete Helmholtz operator, and the algorithm converges in a single iteration. The figure shows that without deflation, the number of GMRES iterations increases with β_2. This is because the SLP preconditioner differs more from the discrete operator as β_2 increases (observed in, e.g., [36]). More interestingly, the figure shows that with deflation, the required number of GMRES iterations initially increases but remains constant for $\beta_2 \geq 0.1$. These results confirm the Fourier analysis spectrum in Section 5 and opens promising perspectives on obtaining a good preconditioner at low cost.

7.2. *One-dimensional constant wavenumber problem*

In Figure 9, we plotted the number of SLP preconditioned GMRES iterations with and without deflation required to solve the one-dimensional Helmholtz on the interval $(0, 1)$ supplied with

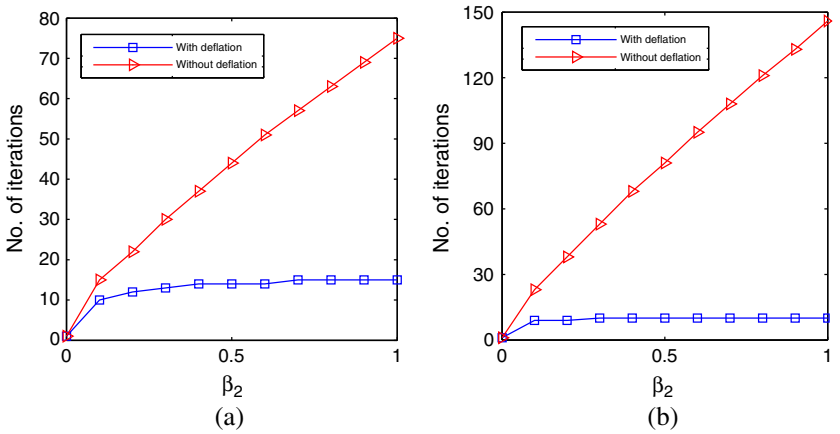

Figure 8. Number of $M_{h,(1,\,\beta_2)}$ preconditioned GMRES iterations with and without deflation versus β_2 for Problem 1 for $k = 50$ and Problem 2 for $f = 30$, both problems with Sommerfeld boundary conditions. (a) Two-dimensional constant wavenumber problem and (b) two-dimensional wedge problem.

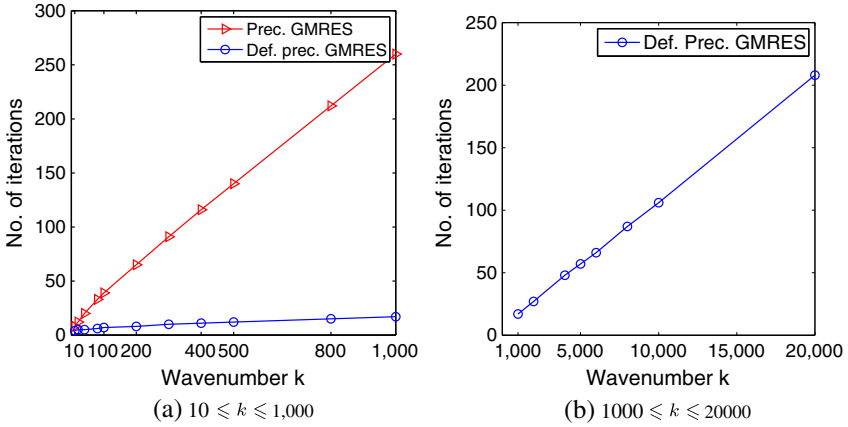

Figure 9. Number of $M_{h,(1,\,1)}$ preconditioned GMRES iterations with and without deflation for the one-dimensional constant wavenumber problem for k ranging (a) between 10 and 1000 and (b) between 1000 and 20,000.

DOI: 10.1002/nla

Sommerfeld boundary conditions. We used the shift $(\beta_1, \beta_2) = (1, 1)$ and 20 grid points per wavelength. In Figure 9(a) and (b), we consider the wavenumber in the range of $0 \leqslant k \leqslant 1000$ and $1000 \leqslant k \leqslant 20,000$, respectively. This figure shows that in the low wavenumber range up to $k = 1000$, the number of iterations is almost independent of k. Starting at $k = 1000$, however, we observed a number of iterations that scales linearly with the wavenumber.

7.3. Two-dimensional constant wavenumber problem

In Figure 10, we plotted the spectrum of the SLP preconditioned operator $S_{h,(1,\,1)}$ and two-grid operator $B_{h,H,(1,\,1)}$ for the constant wavenumber problem (Problem 1) for $k = 50$ with Sommerfeld boundary conditions using 10 grid points per wavelength. In this figure, we used circles to highlight the distance of the cluster of eigenvalues to the origin. Comparing Figure 10(a) and (b) with their equivalues for the Dirichlet boundary conditions in Figure 6 confirms earlier findings in, that is, [36] that the problem with Sommerfeld boundary conditions is easier to solve. This is due to the damping that the boundary conditions introduce. This justifies the use of Dirichlet boundary conditions to analyze the worst-case scenario by Fourier analysis. Figure 10(b) shows that the use of deflation results in a spectrum much more favorable for the convergence of GMRES. Indeed, the cluster of eigenvalues of $B_{h,H,(1,\,1)}$ lies further away from the origin than the spectrum of $S_{h,(1,\,1)}$. How the spectra shown in Figure 10 translate into iteration counts is shown in Tables I and II for various wavenumbers.

In Tables I and II, we give the number of GMRES iterations required to solve the constant wavenumber problem with Dirichlet and Sommerfeld boundary conditions for a range of wavenumbers and number of elements, respectively. We contrast the variants with and without deflation. In both tables, only the number of elements on and below the diagonal highlighted in bold suffice to meet the requirement of 20 mesh points per wavelength, corresponding to $\kappa = 0.3125$. For

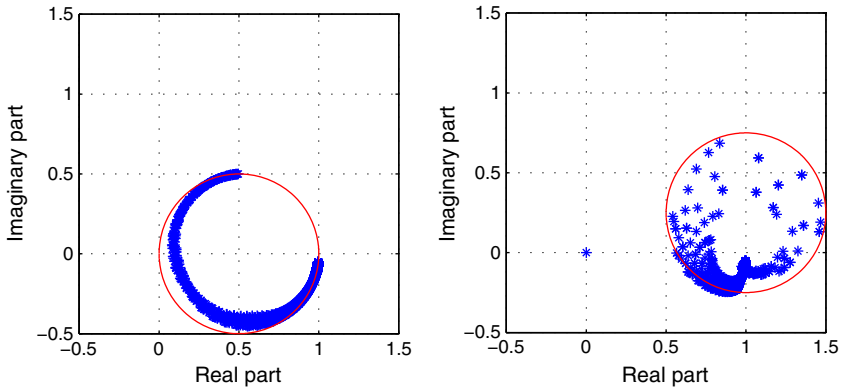

(a) $\sigma(S_{h,(1,.5)})$ (b) $\sigma(B_{h,H,(1,.5)})$

Figure 10. Spectrum of (a) the preconditioned Helmholtz $S_{h,(1,\,0.5)}$ and (b) two-grid preconditioner $B_{h,H,(1,\,0.5)}$ for Problem 1 with Sommerfeld boundary conditions for $\kappa = 0.625$.

Table I. Number of GMRES iterations for Problem 1 with Dirichlet boundary conditions for various wavenumbers and grid resolutions using the SLP preconditioner $M_{h,(1,\,0.5)}$ with and without deflation.

	$k = 10$	$k = 20$	$k = 30$	$k = 40$	$k = 50$	$k = 100$
$n = 32$	**3/10**	8/17	17/31	35/50	52/80	13/14
$n = 64$	3/10	**6/17**	10/30	17/47	24/63	221/252
$n = 96$	3/10	5/17	**7/30**	11/46	15/62	209/220
$n = 128$	3/10	5/17	6/30	**10/45**	11/62	90/196
$n = 160$	3/10	4/17	5/30	8/45	**9/62**	65/194
$n = 320$	2/10	3/17	4/30	5/45	6/61	**24/193**

DOI: 10.1002/nla

Table II. Number of GMRES iterations for Problem 1 with Sommerfeld boundary conditions for various wavenumbers and grid resolutions using the SLP preconditioner $M_{h,(1,\,0.5)}$ with and without deflation.

	$k = 10$	$k = 20$	$k = 30$	$k = 40$	$k = 50$	$k = 100$
$n = 32$	**5/10**	8/17	14/28	26/44	42/70	13/14
$n = 64$	4/10	**6/17**	8/28	12/36	18/45	173/163
$n = 96$	3/10	5/17	**7/27**	9/35	12/43	36/97
$n = 128$	3/10	4/17	6/27	**7/35**	9/43	36/85
$n = 160$	3/10	4/17	5/27	6/35	**8/43**	25/82
$n = 320$	3/10	4/17	4/27	5/35	5/42	**10/80**

both Dirichlet and Sommerfeld boundary conditions, the number of iterations for fixed k decreases with increasing n and thus increasing the number of grid points per wavelength. This confirms our Fourier analysis. The diagonal just above the highlighted one corresponds to $\kappa = 0.625$. For this often used discretization, the growth in the number of iterations is larger than for the case that $\kappa = 0.3125$.

7.4. Two-dimensional wedge problem

In this section, we consider the two-dimensional wedge problem (Problem 2). As in the previous section, we give in Table III the required number of GMRES iterations for various frequencies and mesh sizes with and without deflation. In this table, the leftmost column indicates the number of grid points used in each coordinate direction. This table shows that although deflation is effective in reducing the number of iterations even in the case of nonconstant wavenumbers, not all near-null spaces of the system are sufficiently removed to obtain a fully scalable algorithm. The number of elements on the diagonal highlighted in bold meet the requirement of approximately 20 mesh points per wavelength.

7.5. Multilevel Krylov algorithm

In Table IV, we give the number of outer GCR [37] iterations required to solve Problem 1 using multilevel algorithm ML-ADEF-1 for various values of the wavenumber using 20 grid points per wavelength. We recursively apply coarsening until we obtain a single grid point on the coarsest level.

Table III. Number of $M_{h,(1,\,0.5)}$ preconditioned GMRES iterations with and without deflation for Problem 2 for various wavenumbers and grid resolutions.

	freq = 10	freq = 20	freq = 30	freq = 40	freq = 50
74×124	**7/33**	20/60	79/95	267/156	490/292
148×248	5/33	**9/57**	17/83	42/112	105/144
232×386	5/33	7/57	**10/81**	25/108	18/129
300×500	4/33	6/57	8/81	**12/105**	18/129
374×624	4/33	5/57	7/80	9/104	**13/128**

Table IV. Number of outer GCR iterations preconditioner by ML-ADEF-1 for Problem 1 for various wavenumbers and $\kappa = 0.3125$ using the shifts $(\beta_1, \beta_2) = (1,\ 1)$.

	$k = 10$	$k = 20$	$k = 40$	$k = 80$	$k = 160$
TL	6	7	11	15	25
ML-ADEF-1(4,2,1)	9	11	16	27	100+
ML-ADEF-1(6,2,1)	9	10	14	21	47
ML-ADEF-1(8,2,1)	9	10	13	20	38
ML-ADEF-1(8,3,2)	9	10	13	19	37
ML-ADEF-1(10,2,1)	9	10	14	19	32

DOI: 10.1002/nla

In Table IV, the abbreviation TL stands for the two-level algorithm considered before, whereas the indices n_1, n_2, and n_3 in the notation ML-ADEF-1($n_1, n_2,$ and n_3) denote the number of GCR iterations on the first, second, and third coarser levels, respectively. On the next coarser levels, a single GCR iteration is used, except for the coarsest level where a direct solver is employed. A single standard V(1, 1)-cycle with damped Jacobi used as a damping parameter and $\omega = 2/3$ as a smoother was used to approximate the SLP preconditioner. Table IV shows that obtaining scalability in the range of wavenumbers considered requires increasing n_1 (the number of GMRES iterations on the first coarser level), indicating again that the solver considered is not scalable.

8. CONCLUSIONS

In this paper, we performed a rigorous Fourier analysis of a two-level variant of the multilevel Krylov method for the Helmholtz equation proposed in [1]. The distinct feature of the solver analyzed is the two-level deflation of the SLP at each step of an outer Krylov subspace acceleration. Our analysis of one-dimensional and two-dimensional models reveals three properties of the solver. The first is that with deflation, the solver performs better than without deflation for medium-sized wavenumber problems. Beyond a certain threshold value, however, the solver depends again linearly on the wavenumber. The second property is that the SLP can be made arbitrarily diagonally dominant by increasing the imaginary part of the shift without paying any penalty in the number of Krylov iterations. The third property is that with the use of deflation, the required number of shifted Laplacian iterations decreases with an increasing number of grid points per wavelength. These properties are verified by numerical experiments on constant and nonconstant wavenumber problems and will be exploited in the future in tackling large-scale problems.

ACKNOWLEDGEMENT

We sincerely thank two anonymous reviewers for their comments on a previous draft of the paper allowing us to make several improvements.

REFERENCES

1. Erlangga YA, Nabben R. On a multilevel Krylov method for the Helmholtz equation preconditioned by shifted Laplacian. *Electronic Transactions on Numerical Analysis (ETNA)* 2008; **31**:403–424.
2. Brandt A, Livshitz I. Ray wave multigrid method for Helmholtz equation. *Electronic Transactions on Numerical Analysis (ETNA)* 1997; **6**:162–181.
3. Elman HC, Ernst OG, O'Leary DP. A multigrid method enhanced by krylov subspace iteration for discrete Helmholtz equations. *SIAM Journal on Scientific Computing* April 2001; **23**(4):1291–1315.
4. Haber E, MacLachlan S. A fast method for the solution of the Helmholtz equation. *Journal of Computational Physics* June 2011; **230**(12):4403–4418.
5. Engquist B, Ying L. Sweeping preconditioner for the Helmholtz equation: hierarchical matrix representation. *Communications on Pure and Applied Mathematics* 2011; **64**(5):697–735.
6. Erlangga YA. Advances in iterative methods and preconditioners for the Helmholtz equation. *Archives of Computational Methods in Engineering* 2008; **15**:37–66.
7. Goldstein CI, Bayliss A, Turkel E. An iterative method for the Helmholtz equation. *Journal of Computational Physics* 1983; **49**:443 –457.
8. Laird LA, Giles MB. Preconditioned iterative solution of the 2D Helmholtz equation. *Technical Report*, Oxford University Mathematical Insitute, Numerical Analysis group, 2002. NA-02/12.
9. Mardoche MMM. Incomplete factorization-based preconditionings for solving the Helmholtz equation. *International Journal for Numerical Methods in Engineering* 2001; **50**:1077–1101.
10. Erlangga YA, Vuik C, Oosterlee CW. On a class of preconditioners for solving the Helmholtz equation. *Applied Numerical Mathematics* 2004; **50**(3-4):409–425.
11. Erlangga YA, Oosterlee CW, Vuik C. A novel multigrid based preconditioner for heterogeneous Helmholtz problems. *SIAM Journal on Scientific Computing* 2006; **27**:1471–1492.
12. Erlangga YA, Vuik C, Oosterlee CW. Comparison of multigrid and incomplete LU shifted-Laplace preconditioners for the inhomogeneous Helmholtz equation. *Applied Numerical Mathematics* 2006; **56**:648–666.
13. Reps B, Vanroose W, Bin Zubair H. On the indefinite Helmholtz equation: complex stretched absorbing boundary layers, iterative analysis, and preconditioning. *Journal of Computational Physics* November 2010; **229**:8384–8405.
14. Bollhöfer M, Grote MJ, Schenk O. Algebraic multilevel preconditioner for the Helmholtz equation in heterogeneous media. *SIAM Journal on Scientific Computing* 2009; **31**:3781–3805.

DOI: 10.1002/nla

15. Airaksinen T, Heikkola E, Pennanen A, Toivanen J. An algebraic multigrid based shifted-Laplacian preconditioner for the Helmholtz equation. *Journal of Computational Physics* 2007; **226**:1196 –1210.
16. Erlangga YA, Nabben R. Deflation and balancing preconditioners for Krylov subspace methods applied to nonsymmetric matrices. *SIAM Journal on Matrix Analysis and Applications* 2008; **30**(2):684–699.
17. Zhu J, Ping XW, Chen RS, Fan ZH, Ding DZ. An incomplete factorization preconditioner based on shifted Laplace operators for FEM analysis of microwave structures. *Microwave and Optical Technology Letters* 2010; **52**:1036–1042.
18. Airaksinen T, Pennanen A, Toivanen J. A damping preconditioner for time-harmonic wave equations in fluid and elastic material. *Journal of Computational Physics* March 2009; **228**:1466–1479.
19. Riyanti CD, Kononov A, Erlangga YA, Vuik C, Oosterlee C, Plessix RE, Mulder WA. A parallel multigrid-based preconditioner for the 3D heterogeneous high-frequency Helmholtz equation. *Journal of Computational Physics* 2007; **224**:431–448.
20. Plessix RE. A Helmholtz iterative solver for 3D seismic-imaging problems. *Geophysics* 2007; **72**:SM185–SM194.
21. Plessix RE. Three-dimensional frequency-domain full-waveform inversion with an iterative solver. *Geophysics* 2009; **74**(6):149–157.
22. Umetani N, MacLachlan SP, Oosterlee CW. A multigrid-based shifted Laplacian preconditioner for a fourth-order Helmholtz discretization. *Numerical Linear Algebra with Applications* 2009; **16**:603–626.
23. Airaksinen T, Mönkölä S. Comparison between the shifted-Laplacian preconditioning and the controllability methods for computational acoustics. *Journal of Computational and Applied Mathematics* July 2010; **234**:1796–1802.
24. Osei-Kuffuor D, Saad Y. Preconditioning Helmholtz linear systems. *Applied Numerical Mathematics* April 2010; **60**:420–431.
25. Calandra H, Gratton S, Lago R, Pinel X, Vasseur X. Two-level preconditioned Krylov subspace methods for the solution of three-dimensional heterogeneous Helmholtz problems in seismics. *Numerical Analysis and Applications* 2012; **5**:175–181.
26. van Gijzen MB, Erlangga YA, Vuik C. Spectral analysis of the discrete Helmholtz operator preconditioned with a shifted Laplacian. *SIAM Journal on Scientific Computing* 2007; **29**:1942–1958.
27. Cools S, Vanroose W. Local Fourier analysis of the complex shifted laplacian preconditioner for Helmholtz problems. *Numerical Linear Algebra with Applications* 2013; **20**(4):575–597.
28. Erlangga YA, Nabben R. Algebraic multilevel Krylov methods. *SIAM Journal on Scientific Computing* 2009; **31**:3417–3437.
29. Tang JM, MacLachlan SP, Nabben R, Vuik C. A comparison of two-level preconditioners based on multigrid and deflation. *SIAM Journal on Matrix Analysis and Applications* 2010; **31**:1715–1739.
30. Tang JM. Two level preconditioned conjugate gradient methods with applications to bubbly flow problems. *Ph.D. Thesis*, DIAM, TU Delft, 2008.
31. Pestana J, Wathen AJ. On choice of preconditioner for minimum residual methods for nonsymmetric matrices. *Report na10-07,. Technical Report*, Oxford University Mathematical Insitute, Numerical Analysis group, 2010.
32. Plessix RE, Mulder WA. Separation-of-variables as a preconditioner for an iterative Helmholtz solver. *Applied Numerical Mathematics* 2003; **44**:385–400.
33. Bayliss A, Goldstein CI, Turkel E. On accuracy conditions for the numerical computation of waves. *Journal of Computational Physics* 1985; **59**(3):396–404.
34. Saad Y, Schultz MH. GMRES: a generalized minimal residual algorithm for solving nonsymmetric linear systems. *SIAM Journal on Scientific and Statistical Computing* 1986; **7**(3):856–869.
35. van der Vorst HA. Bi-CGSTAB: a fast and smoothly converging variant of Bi-CG for the solution of nonsymmetric linear systems. *SIAM Journal on Scientific and Statistical Computing* 1992; **13**(2):631–644.
36. Erlangga YA. A robust and effecient iterative method for numerical solution of Helmholtz equation. *Ph.D. Thesis*, DIAM, TU Delft, 2005.
37. Eisenstat SC, Elman HC, Schultz MH. Variational iterative methods for nonsymmetric systems of linear equations. *SIAM Journal on Numerical Analysis* 1983; **20**(2):345–357.
38. Sheikh AH, Vuik C, Lahaye D. A scalable Helmholtz solver combining the shifted Laplace preconditioner with multigrid deflation. *Technical Report, DIAM Report 11-01*, Delft University of Technology, Delft, 2011.
39. Trottenberg U, Oosterlee CW, Schüller A. *Multigrid.* Academic Press: London, 2000.

DOI: 10.1002/nla